Hindawi
Geofluids
Volume 2023, Article ID 6445995, 16 pages
https://doi.org/10.1155/2023/6445995

Research Article

Supporting Mechanism of Pile-Anchor Systems for Deep Foundation Pits in Alpine Regions during the Spring Thaw

Qiang Shi,[1] Dehui Zhao,[1] Ye Wang,[1] Yufeng Li,[1] Lei Zhu,[2] and Zhihe Cheng[2]

[1]*State Grid East Inner Mongolia Electric Power Company Limited, Hohhot 150100, China*
[2]*School of Civil Engineering, Harbin Institute of Technology, Harbin 150090, China*

Correspondence should be addressed to Zhihe Cheng; 17204054005@stu.xust.edu.cn

Received 16 November 2022; Revised 14 April 2023; Accepted 5 May 2023; Published 20 May 2023

Academic Editor: Zhixiong Zeng

This study investigated the supporting mechanism of the retaining piles and prestressed anchor cables of a deep foundation pit in alpine regions during the spring thaw. A numerical model was developed based on a subway project in Changchun City. Field monitoring data and the numerical model were used to analyze the variations in the ground settlement, horizontal displacement of the pile tops, and axial force of the anchor cables during the spring thaw under different working conditions. The results demonstrated that changes in the ground settlement primarily occurred in the late stages of the spring thaw with no obvious settlement phenomena because of the thaw. The pile top displacement of most piles remained stable. The axial force of the anchor cables gradually decreased and then sharply increased early in the spring thaw and then slowly decreased in the middle and late stages. Increasing the pile length decreased the pile top displacement to a certain point. Moreover, increasing the pile length increased the axial force of the first anchor cable but decreased the axial force of the lower four anchor cables. Furthermore, increasing the pile spacing increased the pile top displacement and axial force of the five anchor cables. Increasing the incident angle of the anchor cables decreased the pile top displacement and increased the axial force of the first, third, and fourth cables. The axial force of the second cable was minimized at an incident angle of 14°, and the axial force of the fifth cable was minimized at incident angles of 16° and 18°.

1. Introduction

In regions with seasonally frozen soil, the air temperature often cycles below and above the freezing point of water during the spring thaw, which accelerates the frequency of changes in the water volume in the soil. For foundation pits in such regions, the soil cannot effectively discharge the thawed water, which causes frost heaving and results in severe pressure on the pile-anchor system of the foundation pit [1–3]. Luo et al. reported that freeze thaw cycles increase the internal microporosity of concrete, which causes cracks to accumulate, grow, and eventually lead to concrete failure [4]. Gong et al. suggested adding fibers to improve the cohesion and internal friction angle of concrete, but the effectiveness gradually decreased as the number of freeze thaw cycles increased [5]. Jin et al. established a freeze thaw damage model with fractal dimensions as the independent variable and quantified the relationship between the concrete damage degree, damage parameters, and durability coefficient on the microscale [6]. They conducted experiments and demonstrated that the influence of freeze thaw cycles on interfacial shear behavior could be attributed to water migration and the formation and accumulation of an ice film [7]. Mo and Lou considered the coupling effects of water, heat, force, capillary action, and membrane water migration to study the distribution law of frost heave in the basement soil of a structure with a concrete lining and composite geomembrane [8]. Yuan et al. examined the degradation in

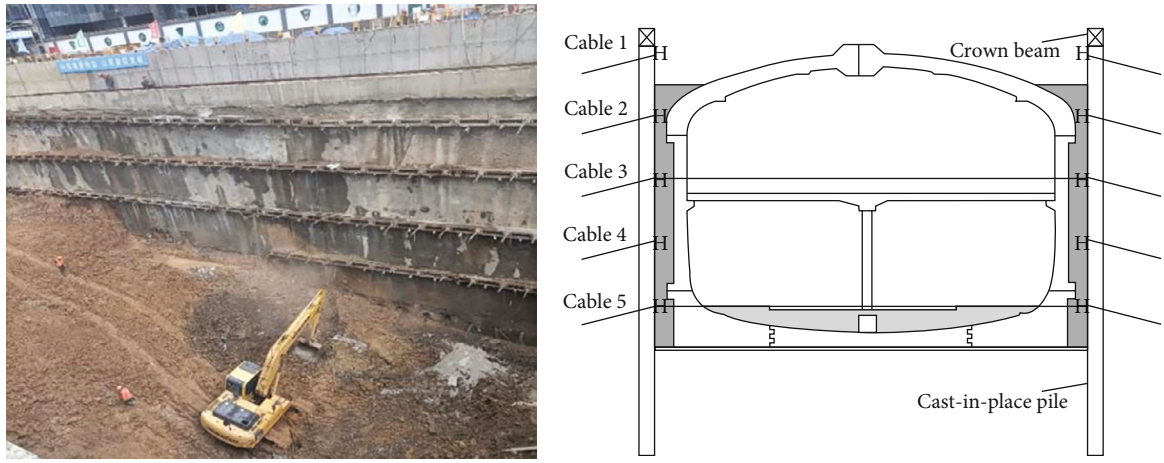

Figure 1: Project overview: (a) construction site and (b) structural profile [19].

Table 1: Design parameters of the prestressed anchor cables.

Anchor cable	Length of anchor cable (m)			Steel strand	Diameter of anchoring body (mm)	Horizontal inclination (°)	Axial force standard value (kN)	Preaxial force (kN)
	Overall length	Length of anchorage section	Length of free section					
First	21.0	13.0	8.0	$3 \times 7\varphi s13.5$	250	15/13	77.8	60
Second	23.0	16.0	7.0	$3 \times 7\varphi s13.5$	250	15/13	169.8	122
Third	27.0	20.0	7.0	$5 \times 7\varphi s13.5$	250	15/13	329.1	244
Fourth	24.0	17.0	7.0	$6 \times 7\varphi s13.5$	250	15/13	453.1	325
Fifth	15.0	10.0	5.0	$5 \times 7\varphi s13.5$	250	15/13	312.0	256

anchoring performance of grouted bolts subjected to freeze thaw cycles and established a model [9]. They observed that the maximum anchoring stress occurred in the middle of the bolts, where shear failure possibly occurs. Liu et al. studied the damage to the shotcrete microstructure because of freeze thaw cycles and its evolution law [10]. Cui et al. demonstrated that the temperature field and mechanical properties of a reinforced retaining wall depend on the ambient temperature and number of freeze thaw cycles [11]. In particular, the top settlement and horizontal displacement of the retaining wall increased with the number of freeze thaw cycles. Li et al. performed a number of tests to study the frost heave mechanism of saturated coarse-grained soil with different fine grain contents and proposed a finite element model based on the Takashi equation [12]. Zhan et al. analyzed the variations in the temperature field, liquid water migration, solid ice accumulation, and frost heave deformation of frozen soil slopes [13]. Dong and Yu proposed a numerical model to simulate the frost heave and stress of water pipes and performed experiments to confirm the reliability of the model at simulating the temperature distribution and volume variation [14]. Chou et al., Zhao et al., Han et al., and Feng et al. used the software Geo-Studio and demonstrated that the thawing depth of slopes subjected to freeze thaw cycles increased with the freezing depth and that a closed loop isotherm formed on the slope [15–19]. Other researchers have used onsite monitoring, indoor freeze thaw tests, thermal parameter tests, and numerical simulations to examine embankments, cut slopes, rock masses, and tunnels in cold regions [20–30].

However, there has been little research on the reliability of a retaining system comprising piles and prestressed anchor cables for deep foundation pits in seasonally frozen regions both at home and abroad. Moreover, the evolution law for the deformation of the retaining piles and axial force of the prestressed anchor cables is not clear. Thus, the design method for pile-anchor systems of deep foundation pits in cold regions with seasonally frozen soil lacks a rational and scientific basis. To address this gap in the literature, this study focused on a construction project for a subway station in Changchun City. Field monitoring data and numerical simulations were used to consider the coupled effects of water, heat, and forces on the foundation pit and clarify the supporting mechanism of the pile-anchor system during the spring thaw.

2. Materials and Methods

2.1. Site Overview. The subway station is located in Changchun, Jilin Province. The station has a length of 245.7 m, standard section width of 20.5 m, and buried depth for the

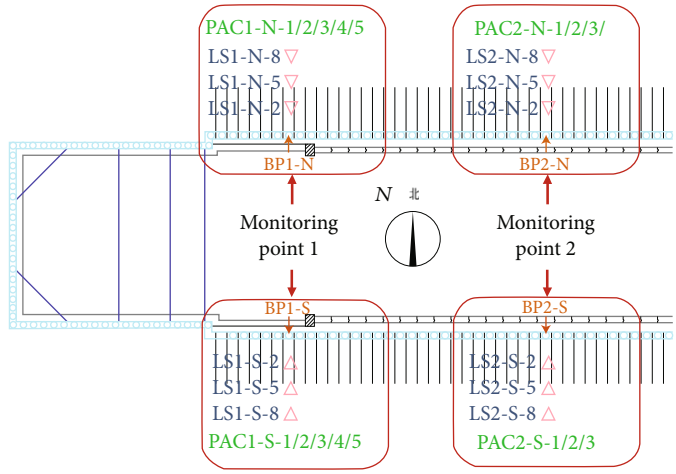

Figure 2: Layout of site measurement points.

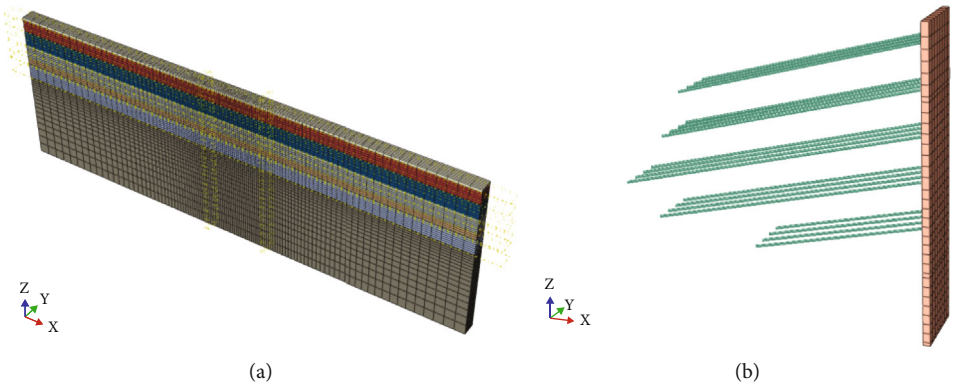

(a) (b)

Figure 3: Three-dimensional numerical model: (a) soil and (b) pile-anchor system [19].

floor of 19.1 m. The foundation pit was excavated from top to bottom through layers of silty clay (average thickness: 15.3 m), fully weathered sandstone (average thickness: 2.4 m), highly weathered mudstone (average thickness: 6.1 m), and medium weathered mudstone (average thickness: 34.3 m). The stable water level had a buried depth of 3.44~4.90 m and elevation of 221.53~222.67 m. The foundation pit had a length of 240.5 m, width of 22.9 m, and excavation depth of 19.7~20.1 m. The retaining structure for the standard section of the foundation pit combined bored cast-in-place piles with prestressed anchor cables, and the retaining structure at both ends of the foundation pit combined bored cast-in-place piles with steel pipes as internal support. The piles had a diameter of 800 mm, length of 25 m, and spacing of 1.3 m. The retaining structures were built using C35 concrete and HRB400 steel reinforcement, as shown in Figure 1 [19].

The anchor cables were anchored into the stable rock mass, and the free ends were fixed between the retaining piles with anchorage. Five anchor cables were set from top to bottom between the piles, and the horizontal spacing of the anchor cables was 1.3 m. The anchor cables comprised twisted steel strands with a standard tensile strength of 1860 MPa. Table 1 presents the design parameters. Changchun City has a temperate continental semihumid to semiarid monsoon climate, and the spring thaw takes place from March to May.

To examine the variations in deformation and stress of the pile-anchor system during the spring thaw, four parameters were monitored: the site temperature, surface settlement, pile top displacement, and axial force of the anchor cables. Figure 2 shows the layout of the measurement points. The measurement points for the surface settlement were symmetrically arranged along the south and north sides of the foundation pit. On each side, the distance between measurement points was 10 m. Moreover, the distance between each measurement point and the free surface of the foundation pit was set to 2, 5, or 8 m. The monitoring frequency was about once every 24 h. The measurement points for the pile top displacement were arranged symmetrically along the south and north sides of the foundation pit at the top of the piles. On each side, the distance between measurement points was 10 m. The monitoring frequency was about once every 24 h. The measurement points for the axial force of the

Table 2: Material parameters.

Serial number		Density ρ (kg/m^3)	Poisson's ratio ν	Elasticity modulus E (MPa)	Conductivity λ (W/(m·K))	Specific heat c (J/(kg·K))	Permeability k (m/s)	Internal friction angle (°)	Cohesion force (kPa)
Soil	1	1850	0.30	10	1.61	1510	2.0E-6	24.1	39.94
	2	1950	0.30	25.2	1.62	1520	3.6E-6	24.1	52.56
	3	1980	0.29	27.2	1.44	1670	5.8E-6	27.8	54.89
	4	2020	0.26	46.8	1.71	1440	4.6E-6	27.8	65.45
	5	1970	0.25	40	1.55	1250	5.8E-5	29.5	52.87
	6	2110	0.24	120	1.37	1060	3.5E-6	44.5	105.55
	7	2130	0.21	160	1.42	1120	9.7E-6	54.8	243.32
Underground diaphragm wall		2500	0.2	31000	1.74	920	—	—	—

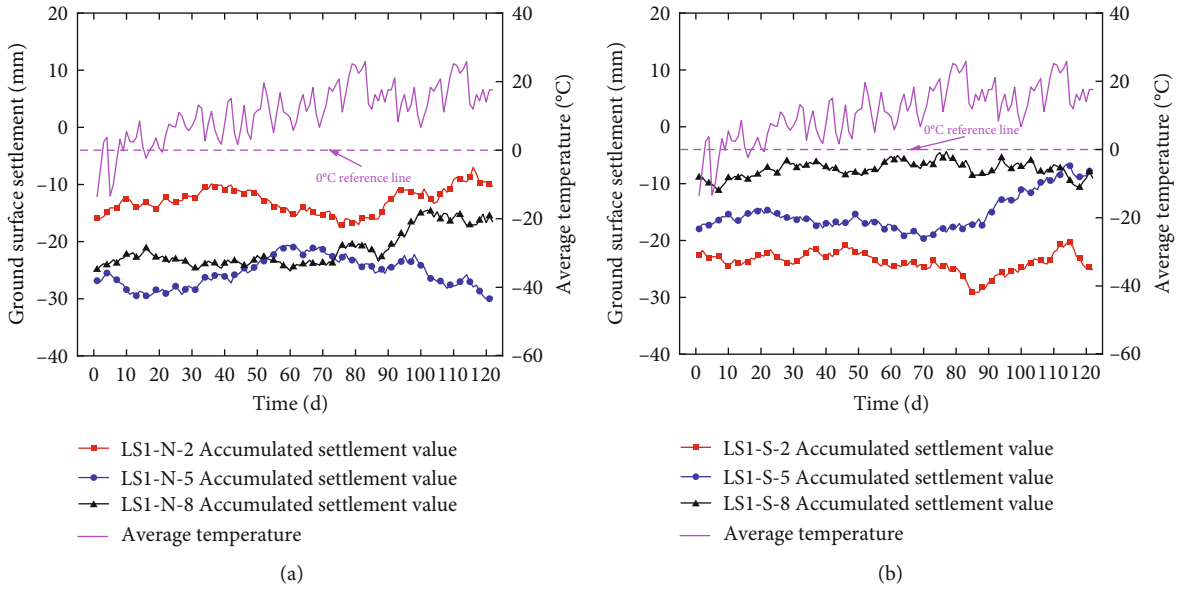

Figure 4: Cumulative settlement of the foundation pit at measurement point 1: (a) north side and (b) south side.

anchor cables were symmetrically arranged along the south and north sides of the foundation pit. On each side, the distance between measurement points was 30 m. Each measurement point monitored the axial forces of 10 anchor cables on the south and north sides of the foundation pit, which corresponded to the cross-section of the measurement point. The monitoring frequency was about once every 24 h, and the measured value and change in the axial force were recorded. The surface subsidence of the bottomless foundation pit was monitored from March to June 2021 at 2, 5, and 8 m from the excavation surface, with a frequency of 24 h. The monitoring points are shown in Figure 2. Measuring points 1 and 2 are located at the north and south sides of the foundation pit and are 2, 5, and 8 m away from the free surface and are denoted as LS(1/2)-(N/S)-(2/5/8).

2.2. Numerical Model. The finite element software ABAQUS was used to establish a 3D numerical model of the pile-anchor structure supporting the foundation pit, as shown in Figure 3 [16]. The model had a length of 182.5 m, width of 5.2 m, and height of 60 m. The piles had a diameter of 0.8 m, length of 25 m, and spacing of 1.3 m, and the crown beam height was 1 m. To facilitate numerical calculation, the bending stiffness equivalent principle was used to simplify the piles into an equal-thickness diaphragm wall. The equivalent thickness of the rear diaphragm wall was calculated to be ~0.486 m. The anchor cables from top to bottom had lengths of 21, 23, 27, 24, and 15 m, respectively. The distances between the anchor cables from top to bottom and the top of the foundation pit were 1.5, 5.0, 8.6, 12.2, and 16.0 m, respectively. The anchor cables had an incident angle of 14°. The modified D-P constitutive model was adopted for the soil, and Table 2 presents the calculated material parameters. An equivalent ground wall was constructed using temperature-displacement coupled 3D solid elements (C3D8T) with an elastic model. The density was 2500 kg/m^3, Poisson's ratio was 0.2, and the elastic modulus was 31 GPa. The prestressed anchor cables were represented by a beam element (B31) and elastic model. The density was 7693 kg/m^3, Poisson's ratio was 0.3, the elastic modulus was 195 GPa, and the expansion coefficient was 1×10^{-5} W/(m · K).

The contact between the ground-linked wall and the soil is selected as face-to-face contact, with the divergent behavior defined by the friction coefficient and the expected behavior set as hard contact. The contact between the prestressing anchor cable and the ground connection wall is achieved through the binding restraint of the free section of the anchor cable to the ground connection wall. In contrast, the contact between the prestressing anchor cable and the soil is achieved through the embedded restraint of the anchor cable anchorage section to the ground.

3. Results and Discussion

3.1. Onsite Monitoring

3.1.1. Surface Settlement. The variation in settlement at the measurement points at different distances from the foundation pit was recorded in March~June 2021. The monitoring data are plotted in Figures 4 and 5. Measurement points 1 and 2 were denoted as LS1 and LS2, respectively. The north and south sides were denoted as N and S, respectively. The distances of 2, 5, and 8 m from the foundation pit were denoted as 2, 5, and 8, respectively. Thus, as an example, the measurement point 1 on the north side and at a distance of 2 m from the foundation pit was denoted as LS1-N-2.

At most measurement points, the change in accumulated settlement primarily occurred late in the spring thaw. This

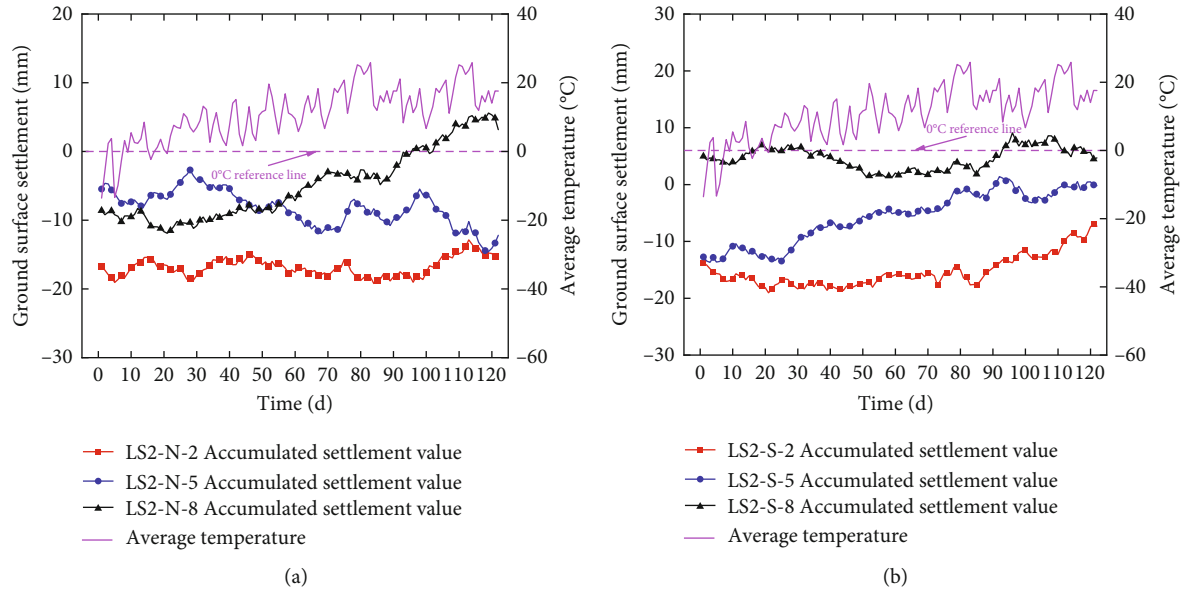

Figure 5: Cumulative settlement of the foundation pit at measurement point 2: (a) north side and (b) south side.

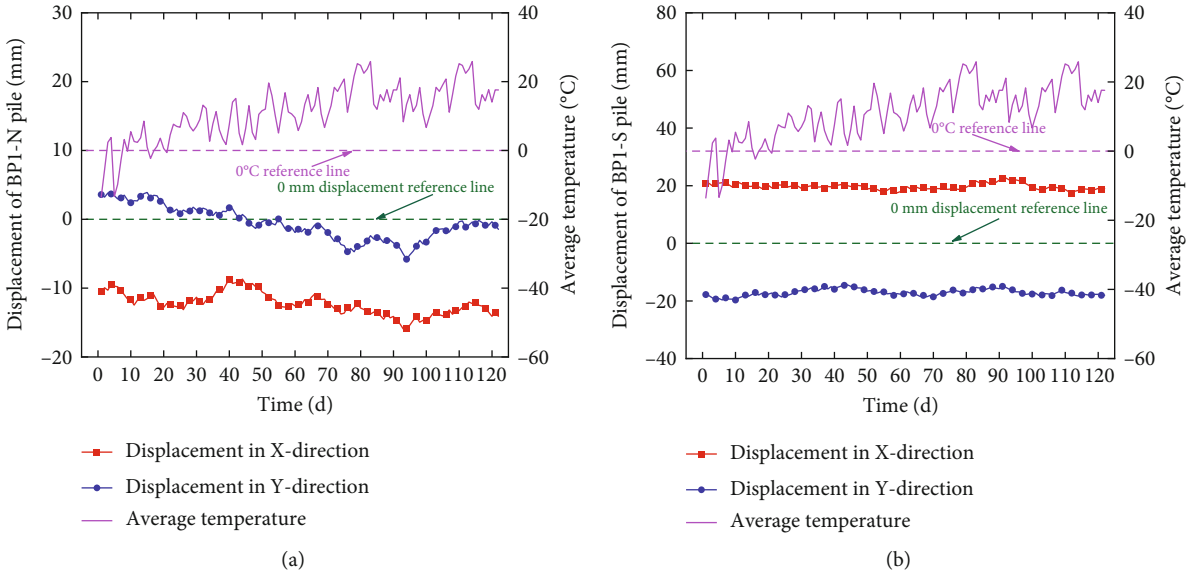

Figure 6: Cumulative displacement of piles in the X and Y directions: (a) BP1-N and (b) BP1-S.

can be attributed to the foundation pit being excavated east of LS1 and the construction that was taking place near LS2. The effect of the excavation had some lag. During the spring thaw, the cumulative settlement was greatest at a distance of 2 m from the open surface, followed by the settlements at 5 and 8 m. Moreover, LS2-N-8 changed from the settlement state to the uplift state late in the spring thaw, while LS2-S-8 was in the uplift state throughout the spring thaw. This may be attributed to asymmetric stacking or dynamic loading in the foundation pit. Early in the spring thaw, the average temperature cycled above 0°C in the afternoon and below 0°C at night. As the soil thawed, water penetrated downward. At night, the soil froze again. Thus, the soil in the foundation pit was subjected to freeze thaw cycles for about a month before thawing fully. However, the accumulated settlement demonstrated no obvious trends early in the spring thaw. The top surface of the foundation pit demonstrated no obvious phenomena throughout the spring thaw.

3.1.2. Pile Top Displacement. The displacement of the retaining piles was monitored in the X and Y directions, and the monitoring data are plotted in Figures 6 and 7. The piles at measurement points 1 and 2 were denoted as BP1 and BP2. The north and south sides of the foundation pit were denoted as N and S. Thus, as an example, the pile at

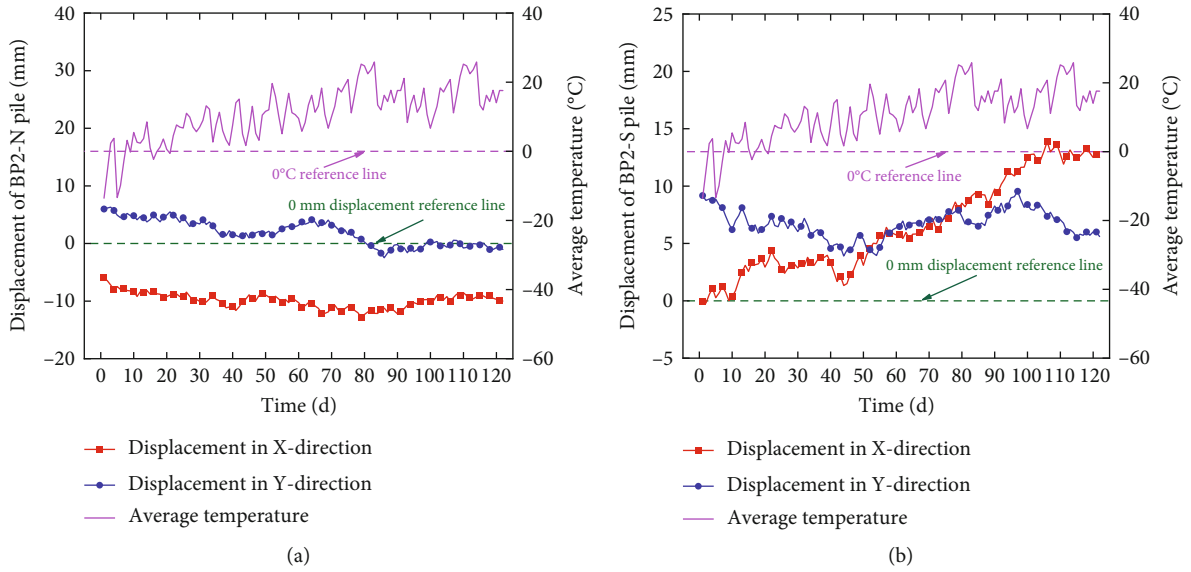

Figure 7: Cumulative displacement of piles in the X and Y directions: (a) BP2-N and (b) BP2-S.

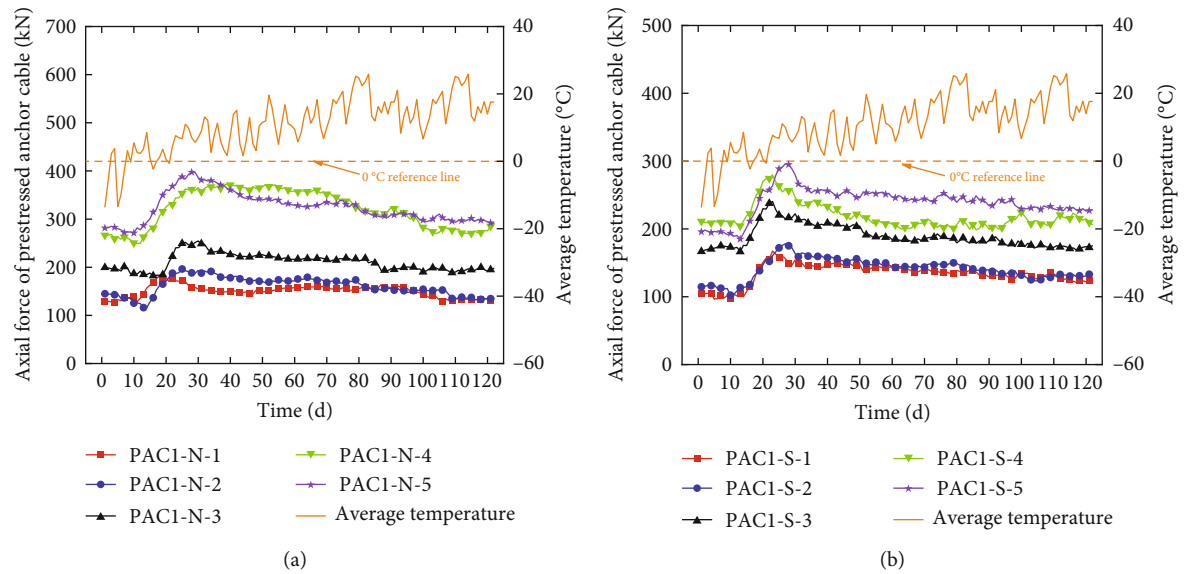

Figure 8: Measured axial force of the anchor cables at measurement point 1: (a) north side and (b) south side.

measurement point 1 on the north side was denoted as BP1-N. The displacement in the X direction is positive in the due east direction and harmful in the standard west order. In contrast, the displacement in the Y direction is set to be positive in the expected north direction and negative in the due south direction.

Except for BP2-S in the X direction, the retaining piles maintained a relatively stable state during the spring thaw. During the spring thaw, the absolute cumulative displacement on the north side of the foundation pit (i.e., BP1-N and BP2-N) was greater in the X direction than in the Y direction. However, the absolute cumulative displacement on the south side (i.e., BP1-S and BP2-S) was similar in the X and Y directions. The X direction displacement on the north side of the foundation pit remained negative (i.e., westward) throughout the spring thaw. Nevertheless, the X direction displacement on the south side remained positive (i.e., eastward) throughout the spring thaw. The Y direction displacement on the north side changed from positive to negative during the spring thaw, and the pile tops gradually moved inside the foundation pit. However, the Y direction displacement on the south side demonstrated different trends. BP1-S demonstrated outward displacement while BP2-S demonstrated inward displacement. Except for BP2-S in the X direction, the cumulative displacement of the piles did not show obvious changes during the early spring thaw

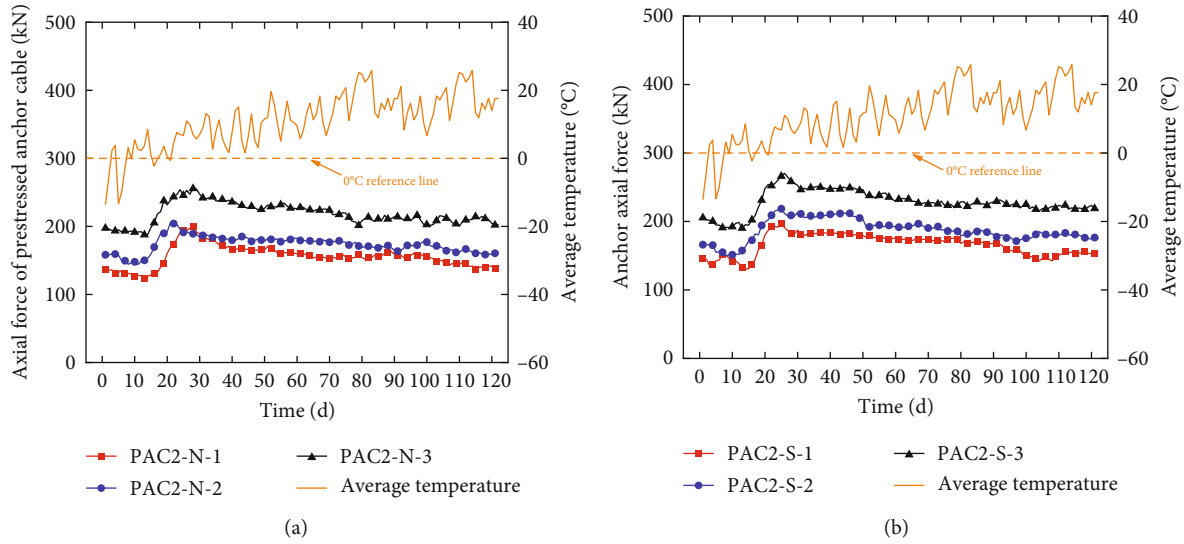

Figure 9: Measured axial force of the anchor cables at measurement point 2: (a) north side and (b) south side.

when freeze thaw cycles were occurring. One possible explanation is that the retaining piles were connected by a crown beam, which may have constrained their horizontal displacements. Furthermore, prestressed anchor cables were being constructed near measurement points 1 and 2, which improved the stability of the retaining pile system. Finally, the pile-anchor system had a better enclosure effect during the spring thaw, which maintained the horizontal pile top displacement in a stable state during the freeze thaw cycles and the spring thaw.

3.1.3. Anchor Cable Axial Force. The variation in the axial force of the anchor cables was monitored at different heights of the same measurement point. The results are shown in Figures 8 and 9. Measurement point 1 (PAC1) had five anchor cables each (1~5) on the north (N) and south (S) sides of the foundation pit, and measurement point 2 (PAC2) had three anchor cables (1~3) each on the north (N) and south (S) sides. Thus, as an example, the first cable at measurement point 1 on the north side was denoted as PAC1-N-1. PAC2 had three cables completed by early March; therefore, only the monitoring data for these three cables were analyzed at this measurement point to ensure data integrity, unlike the five cables monitored at PAC1.

The axial force was similar for all of the anchor cables. The axial force gradually decreased early in the spring thaw, increased sharply, and then decreased. However, the decrease in the axial force demonstrated certain differences among the anchor cables. The axial force of most anchor cables demonstrated a relatively slow decreasing trend in the middle and late stages of the spring thaw. At measurement point 1, the axial force was highest at PAC1-N/S-5, followed by at PAC1-N/S-4, PAC-N/S-3, PAC-N/S-2, and PAC-N/S-1. At measurement point 2, the axial force was highest at PAC2-N/S-3, followed by at PAC2-N/S-2 and PAC2-N/S-1. Thus, the axial force increased from top to bottom.

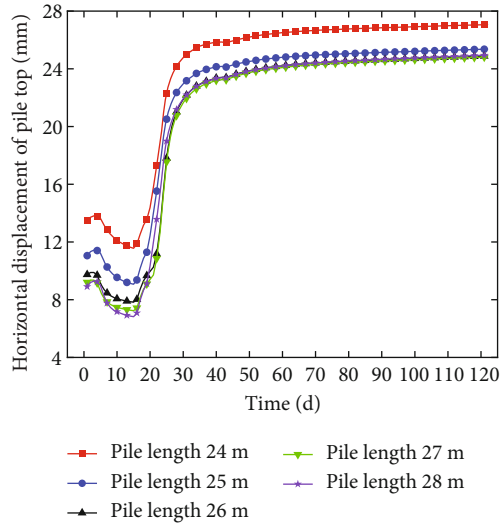

Figure 10: Pile top displacement during the spring thaw with different pile lengths.

Early in the spring thaw, the foundation pit soil experienced freeze thaw cycles for about a month. At this time, the water in the soil behind the pile could not be effectively discharged but accumulated at the boundary between the frozen and unfrozen layers. When the ground temperature at the boundary surface dropped to <0°C, this water refroze, which caused frost heave. This significantly decreased the bearing capacity of the soil and significantly increased the force exerted by the soil on the retaining piles. This further strengthened the movement of the cantilever end of the retaining piles to inside the foundation pit. The horizontal movement of the retaining piles caused tensile deformation of the free ends of the anchor cables that were fixed to the waist beam on the retaining piles. This caused a sudden increase in the axial force of the anchor cables early in the spring thaw. In the middle and late stages of the spring thaw,

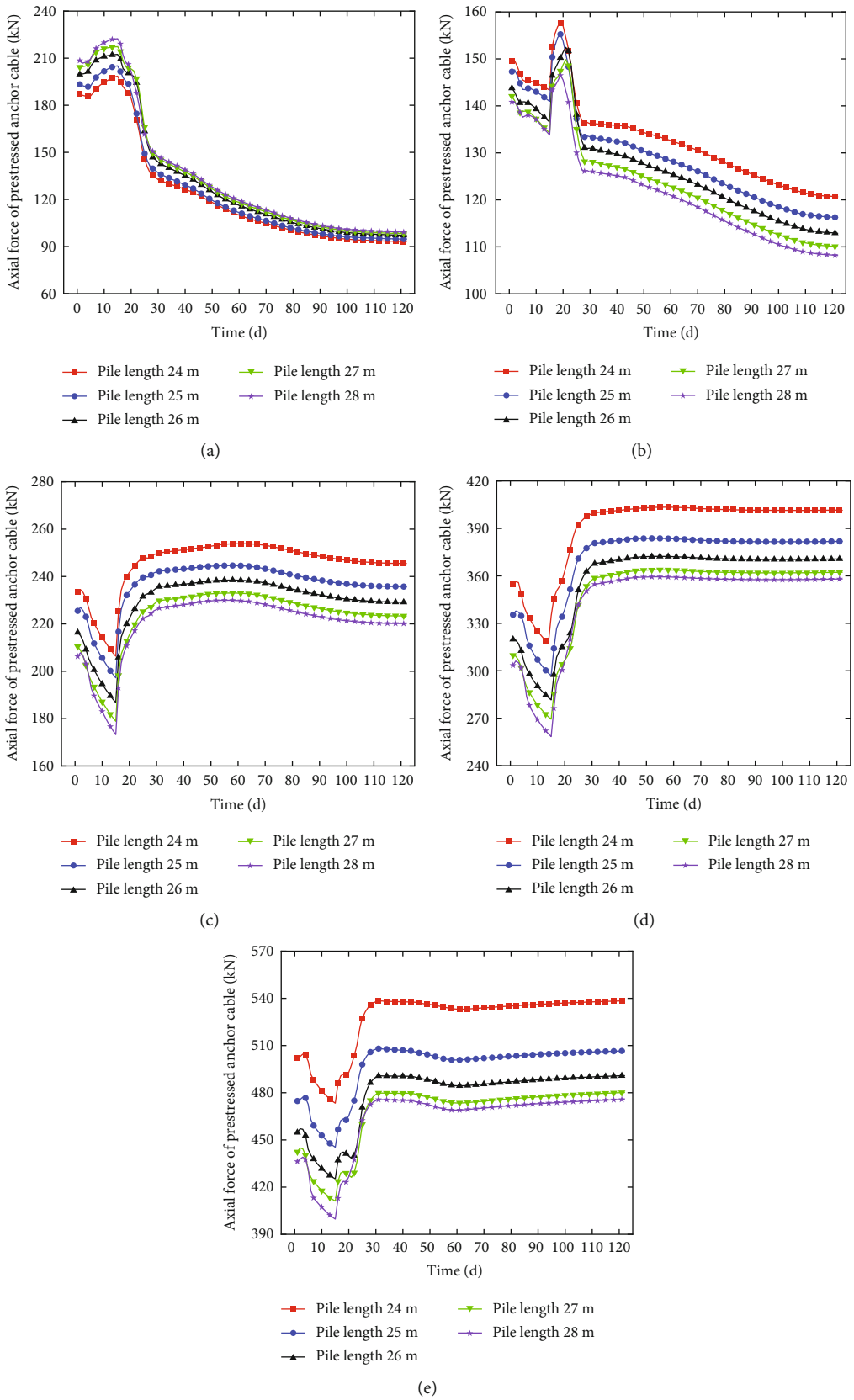

Figure 11: Axial force of anchor cables during the spring thaw with different pile lengths: (a) first, (b) second, (c) third, (d) fourth, and (e) fifth cables.

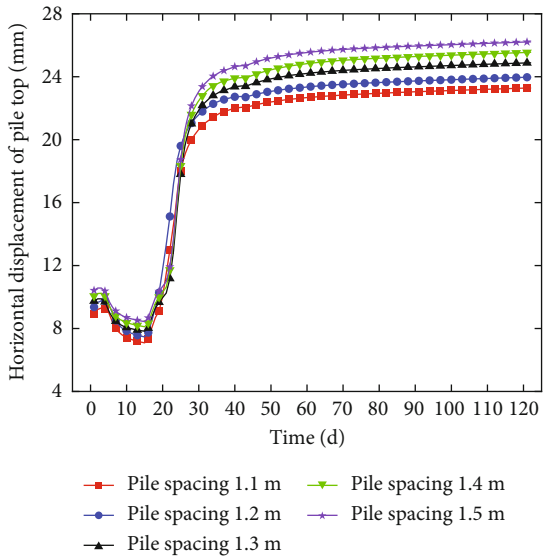

Figure 12: Pile top displacement during the spring thaw with different pile spacings.

the soil was almost completely thawed, and therefore, the soil properties and working state of the pile-anchor system tended to stabilize. Thus, the axial forces of most anchor cables began to slowly decrease.

3.2. Simulation Results

3.2.1. Influence of Pile Length. The 3D numerical model of the pile-anchor system in the deep foundation pit was used to simulate pile lengths of 24, 25, 26 (i.e., actual length), 27, and 28 m. The effects on the horizontal pile top displacement and axial force of the anchor cables were examined. Figure 10 shows the changes in horizontal displacement of the pile tops during the spring thaw. In general, the pile top displacement gradually decreased and then rapidly increased early in the spring thaw, after which it slowly increased in the middle and late stages. The pile top displacement significantly decreased as the pile length was increased from 24 to 25 m and from 25 to 26 m. Increasing the pile length further had no obvious influence on the pile top displacement.

Figure 11 shows the changes in the axial force of five anchor cables during the spring thaw with different pile lengths. The axial force of the first (i.e., topmost) anchor cable initially increased and then rapidly decreased early in the spring thaw. It continued to decrease in the middle stage and then stabilized in the late stage. The axial force of the second anchor cable initially decreased gradually and then sharply increased early in the spring thaw. It then decreased in the middle stage and stabilized in the late stage. The axial forces of the remaining three anchor cables gradually decreased and then increased early in the spring thaw before stabilizing in the middle and late stages.

In the late stage of the spring thaw, changing the pile length had different effects. For the first anchor cable, the axial force gradually increased with an increasing pile length while the variation in the axial force tended to decrease. For the second anchor cable, the axial force gradually decreased with an increasing pile length while the variation in the axial force gradually increased when the pile length was <25 m or >26 m. For the remaining anchor cables, the axial force decreased with an increasing pile length, although the effect weakened with increase in pile length.

3.2.2. Influence of Pile Spacing. The 3D numerical model was used to simulate the effect of varying the pile spacing to 1.1, 1.2, 1.3, 1.4, and 1.5 m. The effects on the horizontal pile top displacement and the axial force of the anchor cables during the spring thaw were studied. Figure 12 shows the changes in the pile top displacement with different pile spacings. The changes were generally consistent with the results for different pile lengths. Increasing the pile spacing gradually increased the pile top displacement. Differences in the pile top displacement gradually increased during the spring thaw when the pile spacing was <1.2 m or >1.3 m. However, the increase in variation was slower when the pile spacing was >1.3 m.

Figure 13 shows the change in axial force of the anchor cables during the spring thaw with different pile spacings. The axial forces of the first, second, and third anchor cables gradually increased with an increasing pile spacing. The amplitude of the variation in the axial force peaked between the pile spacings of 1.2 and 1.3 m. The axial force of the fourth anchor cable gradually increased, and the amplitude of the variation gradually decreased as the pile spacing increased. However, the decrease in the amplitude of the variation was relatively slow when the pile spacing was >1.3 m. The axial force of the fifth anchor cable gradually increased as the pile spacing was increased.

3.2.3. Influence of the Incident Angle of the Anchor Cables. The 3D numerical model was used to simulate the effects of changing the incident angle of the anchor cables to 10°, 12°, 14°, 16°, and 18°. The effects on the pile top displacement

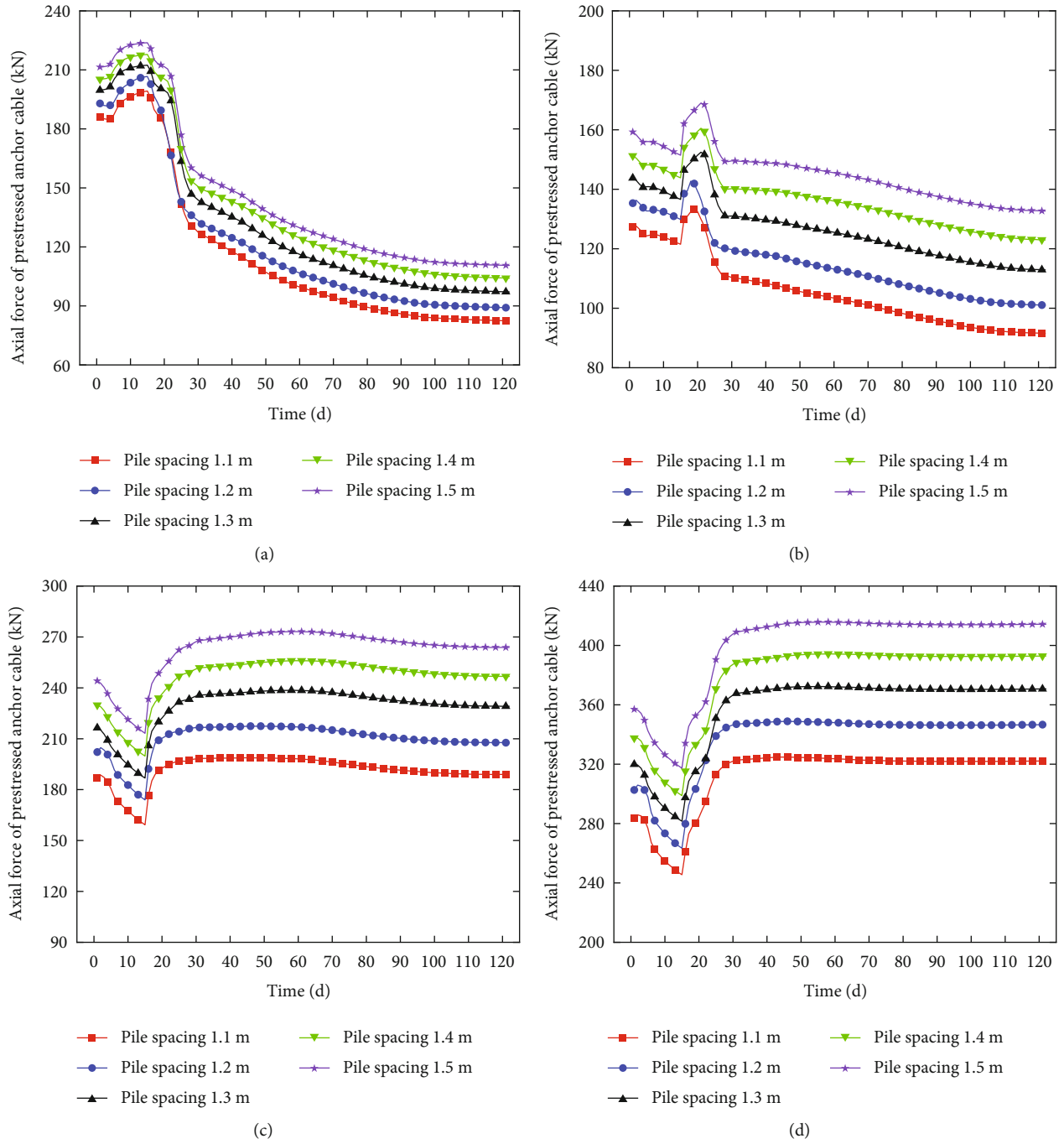

Figure 13: Continued.

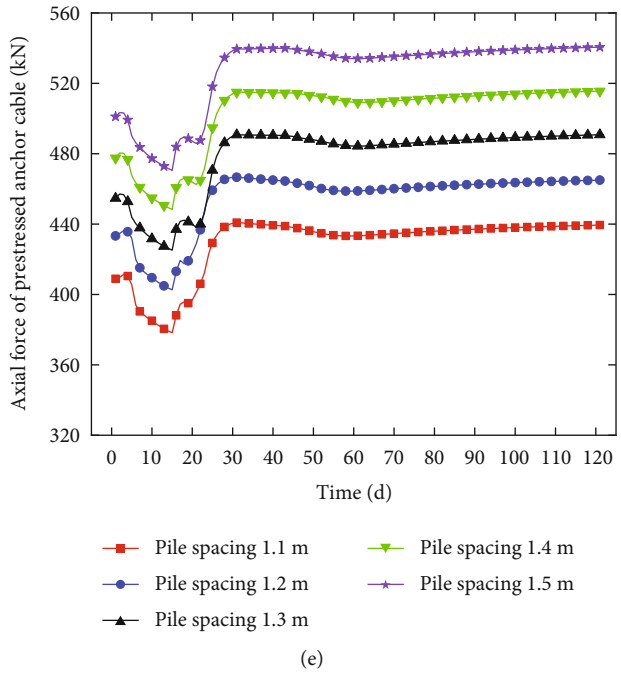

Figure 13: Axial force of anchor cables during the spring thaw with different pile spacings: (a) first, (b) second, (c) third, (d) fourth, and (e) fifth cables.

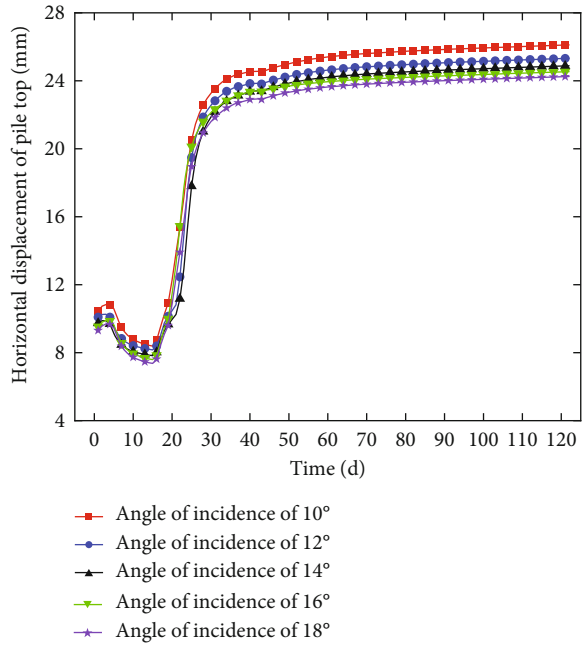

Figure 14: Pile top displacement during the spring thaw with different incident angles of anchor cables.

and the axial force of the anchor cables during the spring thaw were studied. Figure 14 shows the changes in the pile top displacement with different incident angles. The pile top displacement gradually decreased as the incident angle was increased. The difference in the pile top displacement increased gradually during the spring thaw when the incident angle was <14° or >16°. The variation in the pile top displacement was only 0.003% when the incident angle was increased from 14° to 16°. In other words, the amplitude of the variation was minimized between the incident angles of 14° and 16°.

Figure 15 shows the change in axial force of the anchor cables during the spring thaw at different incident angles. The incident angle had different effects on the various anchor cables. The axial forces of the first, third, and fourth anchor cables all increased as the incident angle was

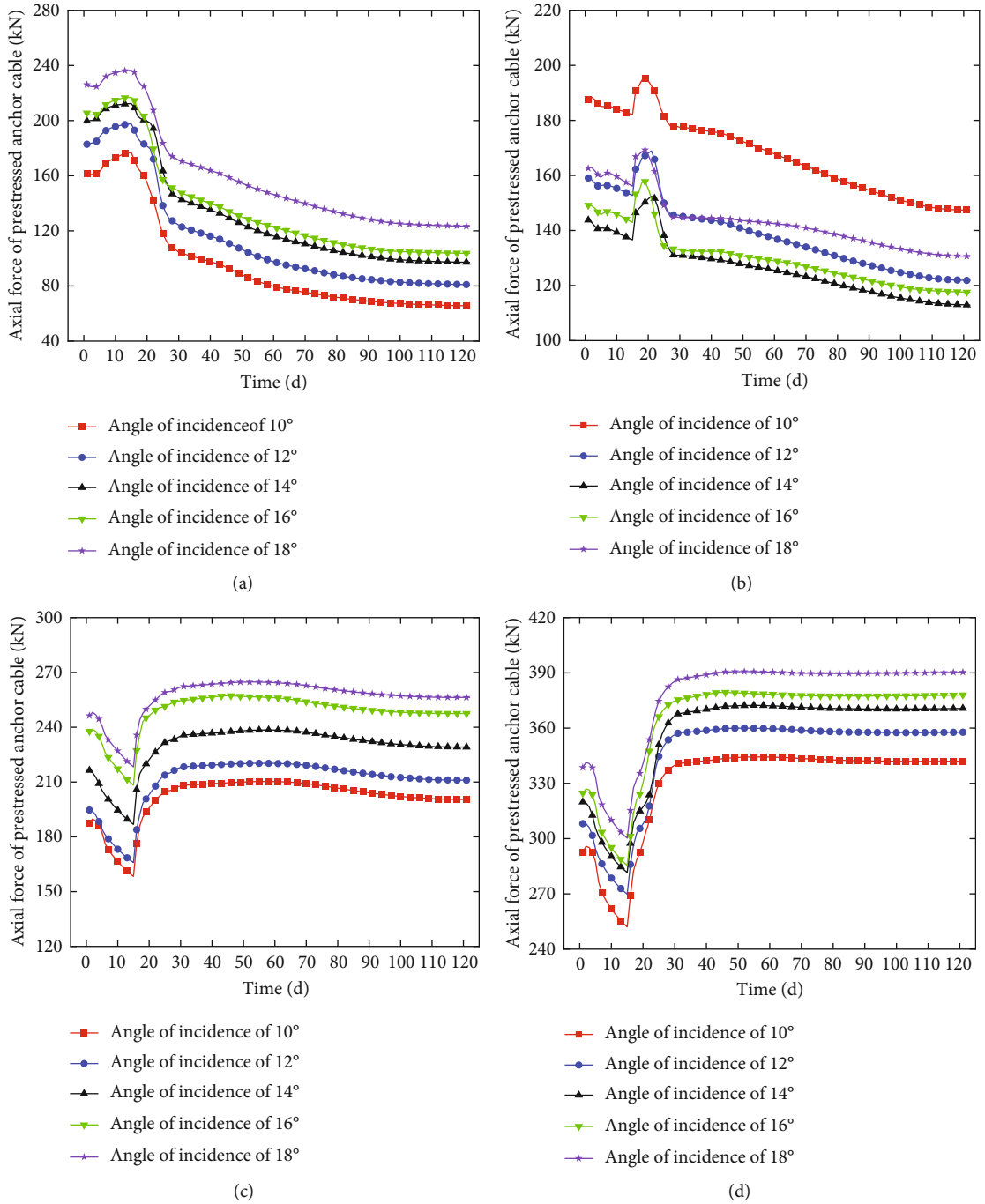

Figure 15: Continued.

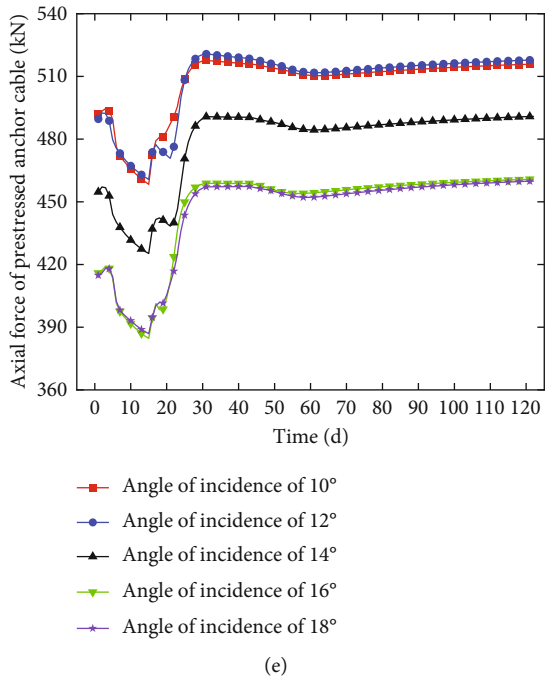

Figure 15: Axial force of anchor cables during the spring thaw with different incident angles: (a) first, (b) second, (c) third, (d) fourth, and (e) fifth anchor cables.

increased. The axial force of the second anchor cable was minimized at an incident angle of 14°. The axial force of the fifth anchor cable was minimized at incident angles of 16° and 18°. The minimum amplitudes of the variation in axial force for the first, second, and fourth anchor cables were possibly at incident angles of 14°~16°. The peak amplitude of the variation in axial force of the third anchor cable was possibly at an incident angle of 12°~16°. The amplitude of the variation in the axial force of the fifth anchor cable was greatest at the incident angles of 12°~16°. The incident angle had a greater effect on the axial force variation of the first and second anchor cables than that of the remaining three anchor cables under the working conditions considered. Therefore, the recommended incident angles for the first, second, third, fourth, and fifth anchor cables are 12°~14°, 14°~16°, 12°~14°, 12°~14°, and 16°~18°, respectively.

4. Conclusions

(1) The cumulative settlement of all measurement points demonstrated no apparent trends during the freeze thaw cycles early in the spring thaw. Most of the changes in compensation occurred late in the spring thaw. There was no significant thawing at the top of the pit throughout the spring thaw. The accumulated pile top displacements demonstrated no apparent trends during the freeze thaw cycles early in the spring thaw, excluding the X direction displacement of BP2-S. The pile top displacements showed relatively stable fluctuations during the spring thaw. BP1-N and BP2-N gradually move from outward movement to inward movement during the spring thaw. Furthermore, BP1-S demonstrated continuous outward movement, while BP2-S demonstrated constant inward movement

(2) The axial forces of all anchor cables demonstrated similar trends. The axial force gradually decreased and then sharply increased early in the spring thaw and then gradually decreased at different rates. In the middle and late stages, most of the anchor cables demonstrated a relatively slow decrease in their axial forces

(3) In the simulation considering pile lengths of 24~28 m, the horizontal pile top displacement decreased as the pile length was increased from 24 to 26 m. Furthermore, increasing the pile length increased the axial force of the first anchor cable but reduced the axial force of the following four anchor cables. Increasing the pile spacing gradually increased the horizontal pile top displacement and the axial force of the five anchor cables. Increasing the incident angle gradually decreased the horizontal pile top displacement and increased the axial forces of the first, third, and fourth anchor cables. The axial force of the second anchor cable was minimized at an incident angle of 14°, and the axial force of the fifth anchor cable was minimized at incident angles of 16° and 18°

Data Availability

The data used to support the findings of this study are included in the article.

Conflicts of Interest

The authors declare that they have no conflicts of interest.

Acknowledgments

This research was supported by the National Natural Science Foundation of China (Grant No. 42101125).

References

[1] Q. Li, Y. Han, X. Liu, U. Ansari, Y. Cheng, and C. Yan, "Hydrate as a by-product in CO_2 leakage during the long-term sub-seabed sequestration and its role in preventing further leakage," *Environmental Science and Pollution Research*, vol. 27, pp. 77737–77754, 2022.

[2] Q. C. Li and J. J. Wu, "Factors affecting the lower limit of the safe mud weight window for drilling operation in hydrate-bearing sediments in the northern South China Sea," *Geomechanics and Geophysics for Geo-Energy and Geo-Resources*, vol. 8, no. 2, 2022.

[3] Q. Li, F. L. Wang, Y. L. Wang et al., "Effect of reservoir characteristics and chemicals on filtration property of water-based drilling fluid in unconventional reservoir and mechanism disclosure," *Environmental Science and Pollution Research*, vol. 30, no. 19, pp. 55034–55043, 2023.

[4] Q. Luo, D. X. Liu, P. Z. Qiao, Q. G. Feng, and L. Z. Sun, "Microstructural damage characterization of concrete under freeze-thaw action," *International Journal of Damage Mechanics*, vol. 27, no. 10, pp. 1551–1568, 2018.

[5] Y. Gong, Y. He, C. Han, Y. Shen, and G. Tan, "Stability analysis of soil embankment slope reinforced with polypropylene fiber under freeze-thaw cycles," *Advances in Materials Science and Engineering*, vol. 2019, Article ID 5725708, 10 pages, 2019.

[6] S. S. Jin, G. P. Zheng, and J. Yu, "A micro freeze-thaw damage model of concrete with fractal dimension," *Construction and Building Materials*, vol. 257, article 119434, 2020.

[7] P. F. He, Y. H. Mu, Z. H. Yang, W. Ma, J. Dong, and Y. Huang, "Freeze-thaw cycling impact on the shear behavior of frozen soil-concrete interface," *Cold Regions Science and Technology*, vol. 173, p. 103024, 2020.

[8] T. F. Mo and Z. K. Lou, "Numerical simulation of frost heave of concrete lining trapezoidal channel under an open system," *Water*, vol. 12, no. 2, p. 335, 2020.

[9] J. K. Yuan, C. W. Ye, J. F. Yang et al., "Experimental and numerical investigation on the deterioration mechanism for grouted rock bolts subjected to freeze-thaw cycles," *Bulletin of Engineering Geology and the Environment*, vol. 80, no. 7, pp. 5563–5574, 2021.

[10] M. X. Liu, D. X. Liu, P. Z. Qiao, and L. Sun, "Characterization of microstructural damage evolution of freeze-thawed shotcrete by an integrative micro-CT and nanoindentation statistical approach," *Cement and Concrete Composites*, vol. 117, p. 103909, 2021.

[11] F. L. Cui, C. Z. Xiao, J. Han, S. Gao, and W. Tian, "Performance of laboratory geogrid-reinforced retaining walls under freeze-thaw cycles," *Geosynthetics International*, vol. 29, no. 1, pp. 81–98, 2022.

[12] Y. Li, F. J. Niu, H. Zheng, S. Akagawa, Z. Lin, and J. Luo, "Experimental measurement and numerical simulation of frost heave in saturated coarse-grained soil," *Cold Regions Science and Technology*, vol. 137, no. 5, pp. 68–74, 2017.

[13] Y. Zhan, Z. Lu, H. Yao, and S. Xian, "A coupled thermo-hydromechanical model of soil slope in seasonally frozen regions under freeze-thaw action," *Advances in Civil Engineering*, vol. 2018, Article ID 7219826, 10 pages, 2018.

[14] S. Dong and X. Yu, "Microstructure-based random finite element method simulation of frost heave: theory and implementation," *Transportation Research Record*, vol. 2672, article 10313420, 2018.

[15] X. F. Lu, F. Zhang, W. J. Qin, H. Zheng, and D. C. Feng, "Experimental investigation on frost heave characteristics of saturated clay soil under different stress levels and temperature gradients," *Cold Regions Science and Technology*, vol. 192, article 103379, 2021.

[16] W. Zhao, J. Y. Han, Y. Chen et al., "A numerical study on the influence of anchorage failure for a deep excavation retained by anchored pile walls," *Advances in Mechanical Engineering*, vol. 10, no. 2, Article ID 168781401875677, 2018.

[17] J. Y. Han, W. Zhao, Y. Chen, P. J. Jia, and Y. P. Guan, "Design analysis and observed performance of a tieback anchored pile wall in sand," *Mathematical Problems in Engineering*, vol. 2017, Article ID 8524078, pp. 1–23, 2017.

[18] J. Y. Han, J. Wang, D. F. Jia et al., "Construction technologies and mechanical effects of the pipe-jacking crossing anchor-cable group in soft stratum," *Frontiers in Earth Science*, vol. 10, article 1019801, 2023.

[19] C. T. Feng, Z. H. Cheng, and L. Lei, "Performance of pre-stressed anchor cables supporting deep foundation pit of a subway station during spring thaw," *Geofluids*, vol. 2022, Article ID 3567816, 14 pages, 2022.

[20] S. Y. Li, Y. M. Lai, M. Y. Zhang, W. Pei, C. Zhang, and F. Yu, "Centrifuge and numerical modeling of the frost heave mechanism of a cold-region canal," *Acta Geotechnica*, vol. 14, no. 4, pp. 1113–1128, 2019.

[21] Y. Ji, G. Zhou, Y. Zhou, and V. Vandeginste, "Frost heave in freezing soils: a quasi-static model for ice lens growth," *Cold Regions Science and Technology*, vol. 158, pp. 10–17, 2019.

[22] S. B. Huang, Y. H. Ye, X. Z. Cui, A. Cheng, and G. Liu, "Theoretical and experimental study of the frost heaving characteristics of the saturated sandstone under low temperature," *Cold Regions Science and Technology*, vol. 174, p. 103036, 2020.

[23] Y. Zhao, J. Feng, K. Liu, H. Xu, L. Wang, and H. Liu, "Study of the stability of a soil-rock road cutting slope in a permafrost region of Hulunbuir," *Advances in Civil Engineering*, vol. 2020, Article ID 6701958, 14 pages, 2020.

[24] J. D. Teng, J. L. Liu, S. Zhang, and D. Sheng, "Modelling frost heave in unsaturated coarse-grained soils," *Acta Geotechnica*, vol. 15, no. 11, pp. 3307–3320, 2020.

[25] C. Qiao, C. H. Li, Y. Wang, H. Yang, and Z. Song, "Research on macro and meso damage model of pre-flawed granites subjected to coupling action of freeze-thaw and loading," *Arabian Journal of Geosciences*, vol. 14, no. 12, pp. 1–14, 2021.

[26] R. Shan, S. Zhang, P. Huang, and W. Liu, "Research on full-section anchor cable and c-shaped tube support system of deep layer roadway," *Geofluids*, vol. 2021, Article ID 5593601, 13 pages, 2021.

[27] A. Fa-you, X.-g. Dai, P. ZHang, M.-c. Hei, and S.-q. Yan, "Experimental investigation of the influence of the anchor cable inclination angle on the seismic response characteristics of anchored piles," *Geofluids*, vol. 2022, Article ID 9167573, 2022.

[28] H. Chen, G. Zhang, Z. Chang, L. Wen, and W. Gao, "Failure analysis of a highway cut slope with anti-slide piles," *Geofluids*, vol. 2021, Article ID 6622214, 2021.

[29] C. Yuan, Z. Hu, Z. Zhu et al., "Numerical simulation of seepage and deformation in excavation of a deep foundation pit under water-rich fractured intrusive rock," *Geofluids*, vol. 2021, Article ID 6628882, 10 pages, 2021.

[30] B. Wang, T. Qin, C. Yuan, L. Li, M. Yuan, and Y. Li, "Analysis of bearing performance of monopile and single suction bucket foundation for offshore wind power under horizontal load," *Geofluids*, vol. 2022, Article ID 4163240, 15 pages, 2022.